Global Budget and Radiative Forcing of Black Carbon Aerosol: Constraints from Pole-to-Pole (HIPPO) Observations across the Pacific

JOURNAL OF GEOPHYSICAL RESEARCH: ATMOSPHERES, VOL. 119, 195–206, doi:10.1002/2013JD020824, 2014

Global budget and radiative forcing of black carbon aerosol: Constraints from pole-to-pole (HIPPO) observations across the Pacific

Qiaoqiao Wang,[1] Daniel J. Jacob,[1,2] J. Ryan Spackman,[3,4] Anne E. Perring,[5,6] Joshua P. Schwarz,[5,6] Nobuhiro Moteki,[7] Eloïse A. Marais,[2] Cui Ge,[8] Jun Wang,[8] and Steven R. H. Barrett[9]

Received 3 September 2013; revised 4 December 2013; accepted 5 December 2013; published 14 January 2014.

[1] We use a global chemical transport model (GEOS-Chem) to interpret aircraft curtain observations of black carbon (BC) aerosol over the Pacific from 85°N to 67°S during the 2009–2011 HIAPER (High-Performance Instrumented Airborne Platform for Environmental Research) Pole-to-Pole Observations (HIPPO) campaigns. Observed concentrations are very low, implying much more efficient scavenging than is usually implemented in models. Our simulation with a global source of 6.5 Tg a^{-1} and mean tropospheric lifetime of 4.2 days (versus 6.8 ± 1.8 days for the Aerosol Comparisons between Observations and Models (AeroCom) models) successfully simulates BC concentrations in source regions and continental outflow and captures the principal features of the HIPPO data but is still higher by a factor of 2 (1.48 for column loads) over the Pacific. It underestimates BC absorbing aerosol optical depths (AAODs) from the Aerosol Robotic Network by 32% on a global basis. Only 8.7% of global BC loading in GEOS-Chem is above 5 km, versus 21 ± 11% for the AeroCom models, with important implications for radiative forcing estimates. Our simulation yields a global BC burden of 77 Gg, a global mean BC AAOD of 0.0017, and a top-of-atmosphere direct radiative forcing (TOA DRF) of 0.19 W m^{-2}, with a range of 0.17–0.31 W m^{-2} based on uncertainties in the BC atmospheric distribution. Our TOA DRF is lower than previous estimates (0.27 ± 0.06 W m^{-2} in AeroCom, 0.65–0.9 W m^{-2} in more recent studies). We argue that these previous estimates are biased high because of excessive BC concentrations over the oceans and in the free troposphere.

Citation: Wang, Q., D. J. Jacob, J. R. Spackman, A. E. Perring, J. P. Schwarz, N. Moteki, E. A. Marais, C. Ge, J. Wang, and S. R. H. Barrett (2014), Global budget and radiative forcing of black carbon aerosol: Constraints from pole-to-pole (HIPPO) observations across the Pacific, *J. Geophys. Res. Atmos.*, *119*, 195–206, doi:10.1002/2013JD020824.

1. Introduction

[2] Black carbon (BC) is of climatic interest as a strong absorber of solar radiation both in the atmosphere [*Jacobson*, 2001; *Koch*, 2001; *Quinn et al.*, 2008] and after deposition to snow [*Warren and Wiscombe*, 1985; *Flanner et al.*, 2007; *McConnell et al.*, 2007]. Estimates of BC radiative forcing have large uncertainties reflecting, in part, poor knowledge of atmospheric concentrations [*Bond et al.*, 2013]. Here we use a global chemical transport model (GEOS-Chem CTM) to interpret aircraft observations of BC from the National Science Foundation HIAPER (High-Performance Instrumented Airborne Platform for Environmental Research) Pole-to-Pole Observations (HIPPO) deployments over the remote Pacific from 85°N to 67°S in 2009–2011. We show that

Additional supporting information may be found in the online version of this article.

[1]School of Engineering and Applied Sciences, Harvard University, Cambridge, Massachusetts, USA.
[2]Department of Earth and Planetary Sciences, Harvard University, Cambridge, Massachusetts, USA.
[3]Science and Technology Corporation, Boulder, Colorado, USA.
[4]Physical Sciences Division, Earth System Research Laboratory, National Oceanic and Atmospheric Administration, Boulder, Colorado, USA.
[5]Chemical Sciences Division, Earth System Research Laboratory, National Oceanic and Atmospheric Administration, Boulder, Colorado, USA.
[6]Cooperative Institute for Research in Environmental Sciences, University of Colorado Boulder, Boulder, Colorado, USA.
[7]Department of Earth and Planetary Science, Graduate School of Science, University of Tokyo, Tokyo, Japan.
[8]Department of Earth and Atmospheric Sciences, University of Nebraska-Lincoln, Lincoln, Nebraska, USA.
[9]Laboratory for Aviation and the Environment, Department of Aeronautics and Astronautics, Massachusetts Institute of Technology, Cambridge, Massachusetts, USA.

Corresponding author: Q. Wang, School of Engineering and Applied Sciences, Harvard University, Pierce Hall, 29 Oxford St., Cambridge, MA 02138, USA. (wang2@fas.harvard.edu)

2169-897X/14/10.1002/2013JD020824

the data provide important constraints on BC radiative forcing, implying that recent estimates of the direct radiative forcing (DRF) may be too high.

[3] DRF at the top-of-atmosphere (TOA DRF) of BC refers to the change in the top-of-atmosphere energy balance due to absorption and scattering of solar radiation by atmospheric BC. Global TOA DRF estimates in the literature range from 0.05 to 1.0 $W m^{-2}$ [*Jacobson*, 2000, 2001; *Schulz et al*., 2006; *Ramanathan and Carmichael*, 2008; *Bond et al*., 2013; *Myhre et al*., 2013], with recent estimates favoring the upper end of that range [*Chung et al*., 2012; *Bond et al*., 2013]. This can be compared to a present-day radiative forcing from CO_2 of 1.82 $W m^{-2}$ in recent Intergovernmental Panel on Climate Change (IPCC) report in 2013 (Working Group I Contribution to the IPCC Fifth Assessment Report Climate Change 2013: The physical science basis: Summary for policymakers, http://www.climatechange2013.org/images/uploads/WGIAR5-SPM_Approved27Sep2013.pdf).

[4] Uncertainty in the global burden and distribution of BC is a major factor of variability in DRF estimates [*Bond et al*., 2013]. Due to limited observations of BC concentrations, particularly in the free troposphere and over the oceans, radiative forcing estimates have been mainly based on model simulations. Estimates by the IPCC report are predominantly based on the AeroCom (Aerosol Comparisons between Observations and Models, http://aerocom.met.no/) ensemble of global models [*Schulz et al*., 2006; *Myhre et al*., 2013]. However, there are order-of-magnitude disagreements between AeroCom models and observations in the remote and upper troposphere [*Koch et al*., 2009; *Schwarz et al*., 2010; *Schwarz et al*., 2013]. This can critically affect DRF estimates [*Zarzycki and Bond*, 2010; *Samset and Myhre*, 2011].

[5] The order-of-magnitude model errors in simulating BC concentrations in the remote troposphere could reflect errors in emission, transport, or wet scavenging which is the main BC sink. Global BC emission inventories such as that from *Bond et al*. [2007] have regional uncertainties of only about a factor of 2–3 as indicated by comparisons with observations in source regions [*Park et al*., 2003; *Koch et al*., 2007; *Wang et al*., 2011; *Fu et al*., 2012; *Leibensperger et al*., 2012]. Evaluation of global models using ^{222}Rn observations shows that transport alone is unlikely to induce errors of much more than a factor of 2 in the remote and upper troposphere [*Jacob et al*., 1997]. Wet scavenging thus appears to be the largest cause of model error in the remote troposphere [*Schwarz et al*., 2010; *Liu et al*., 2011; *Kipling et al*., 2013]. Global models generally use crude parameterizations of the scavenging process [*Balkanski et al*., 1993; *Rasch et al*., 2000]. Additional uncertainties specific to BC scavenging relate to its hydrophilicity [*Park et al*., 2005; *Riemer et al*., 2010; *Liu et al*., 2011] and its potential to serve as cloud condensation nucleus (CCN) or ice nucleus (IN) [*Croft et al*., 2010; *Liu et al*., 2011; *Wang et al*., 2011]. Systematic model errors caused by scavenging will grow with distance from source regions.

[6] Global observations of absorption aerosol optical depth (AAOD) are available from the Aerosol Robotic Network (AERONET) surface network [*Dubovik et al*., 2002] and from satellites [*Remer et al*., 2005; *Torres et al*., 2007]. These have been used to constrain radiative forcing estimates and to evaluate models [*Sato et al*., 2003; *Koch et al*., 2009; *Chung et al*., 2012; *Bond et al*., 2013]. However, their value is limited because of high uncertainty in single-scattering albedo (ω_0) retrievals at low AOD [*Dubovik et al*., 2002], clear-sky bias, and difficulty in distinguishing between BC and other light-absorbing constituents. In addition, AERONET observations are mainly confined to continents, and satellite retrievals are subject to cloud contamination [*Chung et al*., 2005].

[7] Aircraft observations can provide important constraints for the vertical and oceanic distribution of BC. The HIAPER Pole-to-Pole Observations (HIPPO) aircraft program [*Wofsy et al*., 2011] offers a unique resource. It involved near-continuous vertical profiling by the HIAPER aircraft from the surface to 8 km (with occasional forays to 14 km altitude) over the Pacific from 85°N to 67°S. Five deployments were conducted over the 2009–2011 period. Measurements included BC mass concentrations from a single-particle soot photometer (SP2) instrument [*Schwarz et al*., 2010; *Schwarz et al*., 2013] together with a number of gases [*Wofsy et al*., 2011]. Here we present a detailed simulation of the HIPPO BC observations with the GEOS-Chem CTM, examining the constraints that these observations provide on the model representation of scavenging and BC source attribution on a global scale. From there we draw implications for BC radiative forcing. GEOS-Chem has been used before with success to simulate BC observations in source regions [*Park et al*., 2006; *Mao et al*., 2011; *Wang et al*., 2011; *Leibensperger et al*., 2012] as well as vertical profiles from aircraft campaigns in Asian outflow [*Park et al*., 2005], North America [*Drury et al*., 2010] and the Arctic [*Wang et al*., 2011].

2. Model Description

[8] We use the GEOS-Chem CTM version 8-01-04 (http://geos-chem.org) driven by assimilated meteorological data from the Goddard Earth Observing System (GEOS-5) of the NASA Global Modeling and Assimilation Office. The GEOS-5 data have 6 h temporal resolution (3 h for surface quantities and mixing depths), 47 vertical layers, and 0.5° × 0.667° horizontal resolution. We degrade the horizontal resolution to 2° × 2.5° for input to GEOS-Chem. We initialize the model with a 12 year spinup to reach steady state in the stratosphere, followed by simulation of January 2009 to September 2011 for comparison to observations.

[9] The simulation of BC in GEOS-Chem was originally described by *Park et al*. [2003]. BC is emitted by fuel (fossil fuel and biofuel) combustion and open fires. We assume that 80% of freshly emitted BC is hydrophobic [*Cooke et al*., 1999; *Park et al*., 2003] and convert it to hydrophilic with an *e*-folding time of 1 day which yields a good simulation of BC export efficiency in continental outflow [*Park et al*., 2005]. The wet deposition scheme for aerosols in GEOS-Chem was originally described by *Liu et al*. [2001]. In *Wang et al*. [2011], we introduced several improvements, in particular for snow and cold clouds, to simulate ARCTAS (Arctic Research of the Composition of the Troposphere from Aircraft and Satellites) aircraft observations over the Arctic. Here we make further updates to the wet scavenging scheme as described below. Dry deposition is an additional minor sink for BC and its implementation in GEOS-Chem follows a standard resistance-in-series scheme [*Wesely*, 1989] as implemented by *Wang et al*. [1998]. The global annual

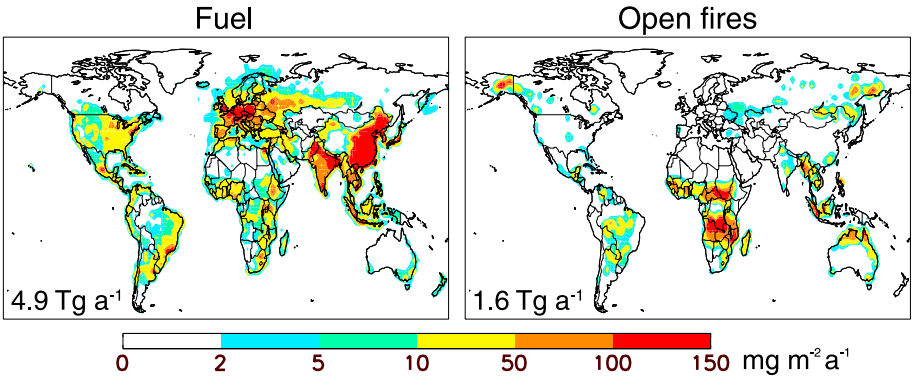

Figure 1. GEOS-Chem annual emissions of black carbon (BC) in 2009, separately for fuel and open fire sources. Global totals are inset.

mean dry deposition velocity for BC in GEOS-Chem is 0.10 cm s^{-1}, typical of current models [*Reddy and Boucher*, 2004; *Huang et al*., 2010].

2.1. Wet Deposition

[10] The standard scheme for aerosol scavenging in GEOS-Chem [*Liu et al*., 2001; *Wang et al*., 2011] includes scavenging in convective updrafts, as well as in-cloud and below-cloud scavenging from anvil and large-scale precipitation. Here we modify the scheme by (1) scavenging hydrophobic aerosol (including hydrophobic BC) in convective updrafts, since this would take place by impaction [*Ekman et al*., 2004], and (2) scavenging water-soluble aerosol (including hydrophilic BC) from cold clouds by homogeneous freezing of solution droplets at $T < 237$ K [*Friedman et al*., 2011].

[11] The GEOS-5 meteorological archive provides 3-D entrainment/detrainment convective mass fluxes with 6-h temporal resolution. These are treated in GEOS-Chem as a single convective updraft for each model grid square. As air rises in the updraft over a distance Δz between two successive model layers, aerosol incorporated in the cloud water is scavenged down to the bottom of the updraft. The fraction f of aerosol mass scavenged from the updraft is given by

$$f = 1 - e^{-\alpha k \Delta z} \quad (1)$$

where k is a coefficient for conversion of cloud water to precipitation with values of $5\text{x}10^{-4}$ m^{-1} over land and 10^{-3} m^{-1} over ocean, and α is the fraction of aerosol mass incorporated in cloud water. In the original scheme of *Liu et al*. [2001] and *Wang et al*. [2011], α accounts for nucleation scavenging and is set to 1 for water-soluble aerosols (excluding hydrophobic BC) at $T \geq 258$ K, and for ice nuclei (IN) at $T < 258$ K. It is set to 0 in other cases. Only dust and hydrophobic BC can serve as IN [*Wang et al*., 2011]. The ability of hydrophobic BC to serve as IN is highly uncertain: some studies find it to be an efficient IN [*Gorbunov et al*., 2001; *Fornea et al*., 2009] but others not [*Koehler et al*., 2009; *Friedman et al*., 2011]. Our assumption here may overestimate the scavenging of hydrophobic BC in cold clouds, but this has little consequence for our purposes since the hydrophobic fraction of BC is very small due to the short *e*-folding time for conversion to hydrophilic in the model.

[12] In our present simulation we set a minimum value of 0.5 for α to account for impaction scavenging. While nucleation scavenging dominates the removal of water-soluble aerosols, impaction scavenging still provides an important mechanism for the removal of hydrophobic aerosols during convective updrafts as indicated by a cloud-resolving model study [*Ekman et al*., 2004]. Similar treatment (in-cloud scavenging ratio of 0.4 for accumulation-mode insoluble aerosols) is used in the aerosol-climate model ECHAM5-HAM [*Croft et al*., 2010]. This update increases removal of hydrophobic aerosols (including hydrophobic BC) but has little effect on water-soluble aerosols which are already efficiently removed by nucleation scavenging.

[13] We also distinguish between homogeneous and heterogeneous freezing nucleation for cold clouds ($T < 258$ K). At $258\text{ K} > T \geq 237$ K, we assume that heterogeneous nucleation dominates ice formation and thus $\alpha = 1$ only for IN ($\alpha = 0.5$ for other aerosols). At $T < 237$ K, we assume that homogeneous nucleation takes place with $\alpha = 1$ for both water-soluble aerosol and IN.

[14] Aerosol scavenging by anvil and large-scale precipitation takes place both in cloud and below cloud in the fraction of the grid box experiencing precipitation. For in-cloud scavenging, the original scheme incorporates all water-soluble aerosols at $T \geq 258$ K or all IN at $T < 258$ K into clouds followed by efficient scavenging when cloud water is converted to precipitation. Now we introduce homogeneous freezing nucleation for in-cloud removal and incorporate 100% of water-soluble aerosol and IN into clouds at $T < 237$ K, same as for convective updrafts. This may overestimate scavenging as updrafts in large-scale clouds are weaker than in deep convection. However, it has little effect in our simulation as the amount of precipitation occurring at $T < 237$ K is very small (see sensitivity simulation in the supporting information). Below-cloud scavenging remains as described by *Wang et al*. [2011].

[15] The above updates improve the simulation of HIPPO data, as shown in the supporting information, without compromising the simulation of other BC data sets as shown below. As the updates also affect simulation of other aerosols, we conducted a ^{222}Rn-^{210}Pb simulation to test the general model representation of aerosol deposition. We find a lifetime of tropospheric ^{210}Pb aerosol against deposition of 8.6 days, as compared to a best estimate of 9 days constrained by observations [*Liu et al*., 2001].

Table 1. Global Emission of Black Carbon in 2009[a]

Source	Emission (Tg C a^{-1})
Fuel[b]	4.9
North America (172.5–17.5°W, 24–88°N)	0.29
Europe (17.5°W–30°E, 50–88°N and 17.5°W–60°E, 33–50°N)	0.63
Russia (30–172.5°E, 50–88°N)	0.22
Asia (60–152.5°E, 0–50°N)	2.7
Australia (90.0–155.0°E, 0–40°S)	0.15
Africa (17.5°W–60.0°E, 35°S–33°N)	0.45
Rest of the world	0.43
Aviation[c]	0.0060
Open Fires[d]	1.6
North America (172.5–17.5°W, 24–88°N)	0.056
Europe (17.5°W–30°E, 33–88°N)	0.0027
Russia (30–172.5°E, 33–88°N)	0.096
South Asia (60–152.5°E, 0–33°N)	0.18
Australia (90.0–155.0°E, 0–40°S)	0.19
Africa (17.5°W–60.0°E, 35°S–33°N)	0.92
Rest of the world	0.13
Total	6.5

[a]Values are annual means. Different regional definitions are used for fuel combustion and open fire sources in Eurasia to improve the model separation between source types.
[b]Including fossil fuel and biofuel. Values are from *Zhang et al.* [2009] for Asia and *Bond et al.* [2007] for the rest of the world but with doubling for Russia and 30% decrease for North America (see text).
[c]AEIC aircraft emission inventory of *Simone et al.* [2013].
[d]GFED3 inventory of *van der Werf et al.* [2010].

2.2. Emissions

[16] Figure 1 shows the global emissions of BC in 2009 in the model, separately for fuel and open fire sources. Table 1 gives regional annual totals. Fuel emissions are from *Bond et al.* [2007] for the year 2000 with modifications for Russia, North America, and Asia. We double the emissions in Russia to account for rapid economic growth since 2000 and as needed to match BC surface observations in the Arctic [*Wang et al.*, 2011]. We decrease North American emissions by 30% to match the observed 2000–2009 decline of surface concentrations in the U.S. [*Leibensperger et al.*, 2012]. For Asia we use the *Zhang et al.* [2009] inventory for 2006, which is 50% higher annually than *Bond et al.* [2007] over China and has greatest difference in winter-spring. Aviation emissions are from *Simone et al.* [2013]. Fire emissions are from the GFED3 (Global Fire Emissions Database version 3) inventory for 2009–2011 with 3 h resolution [*van der Werf et al.*, 2010].

3. Evaluation in Source Regions and Continental Outflow

[17] Before examining model results over the remote Pacific, it is important to evaluate the model sources and export by comparison with observations in source regions and continental outflow. Figure 2 compares annual mean surface air concentrations of BC in the model with network observations from the U.S., China, and Europe. These three regions account for over half of the global fuel BC source. For the U.S., we use 2009 data from the rural IMPROVE (Interagency Monitoring of Protected Visual Environments) network (http://vista.cira.colostate.edu/improve/Data/IMPROVE/AsciiData.aspx). For China and Europe, we do not have network observations for 2009 and therefore use the data for other years: *Zhang et al.* [2008] for rural/regional sites in China in 2006 and the BC/OC campaign in Europe in 2002–2003 (http://tarantula.nilu.no/projects/ccc/emepdata.html).

[18] We diagnose for each source region the normalized mean bias NMB = $\sum(M_i - O_i)/\sum O_i$, where sums are over the ensemble of sites i, and M_i and O_i are the modeled and observed values. NMB values are −27% for China, −28% for Europe, and −12% for the U.S. Underestimation in China mainly occurs in western China, likely associated with underestimates in the use of low-quality fuels for heating [*Fu et al.*, 2012]. For eastern China, the NMB is −13%. Underestimation in Europe is mainly due to 3 (out of 12) sites in northern Italy and Belgium. Without these three sites, the NMB would be +7%.

[19] Figure 3 evaluates the model simulation of continental outflow with aircraft observations through the depth of the troposphere over the U.S., the Pacific Rim, and the Arctic. Observations over the U.S. are from the ensemble of HIPPO data (Figure 4, green lines). Observations for Asian outflow are from the A-FORCE aircraft campaign conducted over the Yellow Sea, the East China Sea, and the western Pacific in March–April 2009 [*Oshima et al.*, 2012]. Observations in

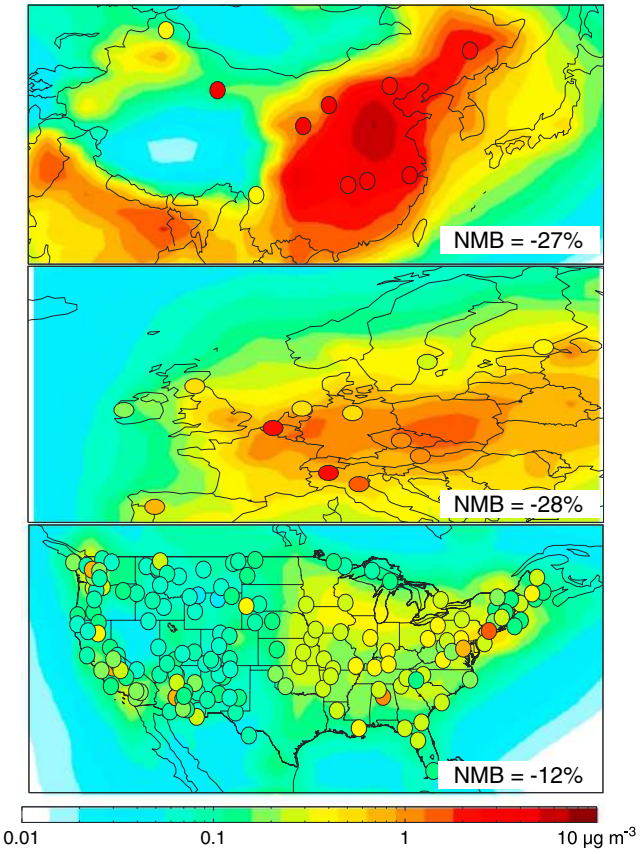

Figure 2. Annual mean surface air concentrations of BC in China, Europe, and the U.S. Model results for 2009 (solid contours) are compared to observations (circles). Observations are from *Zhang et al.* [2008] in China for 2006, from the EMEP network in Europe for 2002–2003 (http://tarantula.nilu.no/projects/ccc/emepdata.html), and from the IMPROVE network in the U.S. for 2009 (http://vista.cira.colostate.edu/improve/Data/IMPROVE/AsciiData.aspx). Normalized mean bias (NMB) statistics for each region are shown inset.

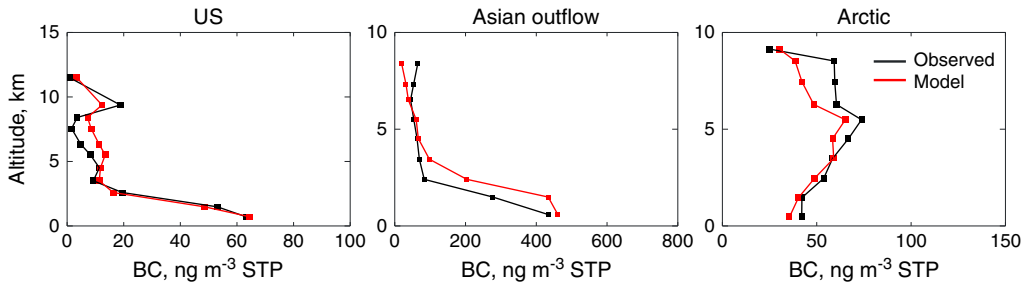

Figure 3. Median vertical profiles of BC concentrations in continental outflow regions. Aircraft observations in 1 km altitude bins (black) are compared to GEOS-Chem model values sampled along the flight tracks (red). The U.S. profile is from the ensemble of HIPPO observations shown as green lines in Figure 4. The Asian outflow profile is from the A-FORCE campaign conducted over the Yellow Sea, the East China Sea, and the western Pacific Ocean in March–April 2009 [*Oshima et al.*, 2012]. Observations in the Arctic are from the ARCTAS campaign in April 2008 as described by *Wang et al.* [2011]. Note differences in linear scales between panels.

the Arctic are from the ARCTAS aircraft campaign in April 2008 [*Jacob et al.*, 2010; *Wang et al.*, 2011]. Observations for individual flights are averaged over the 3-D GEOS-Chem grid, and corresponding model results are sampled along the flight tracks at the same time and location. We then use median of the observed and simulated data in 1 km altitude bins to generate the vertical profiles. We exclude observations in the stratosphere

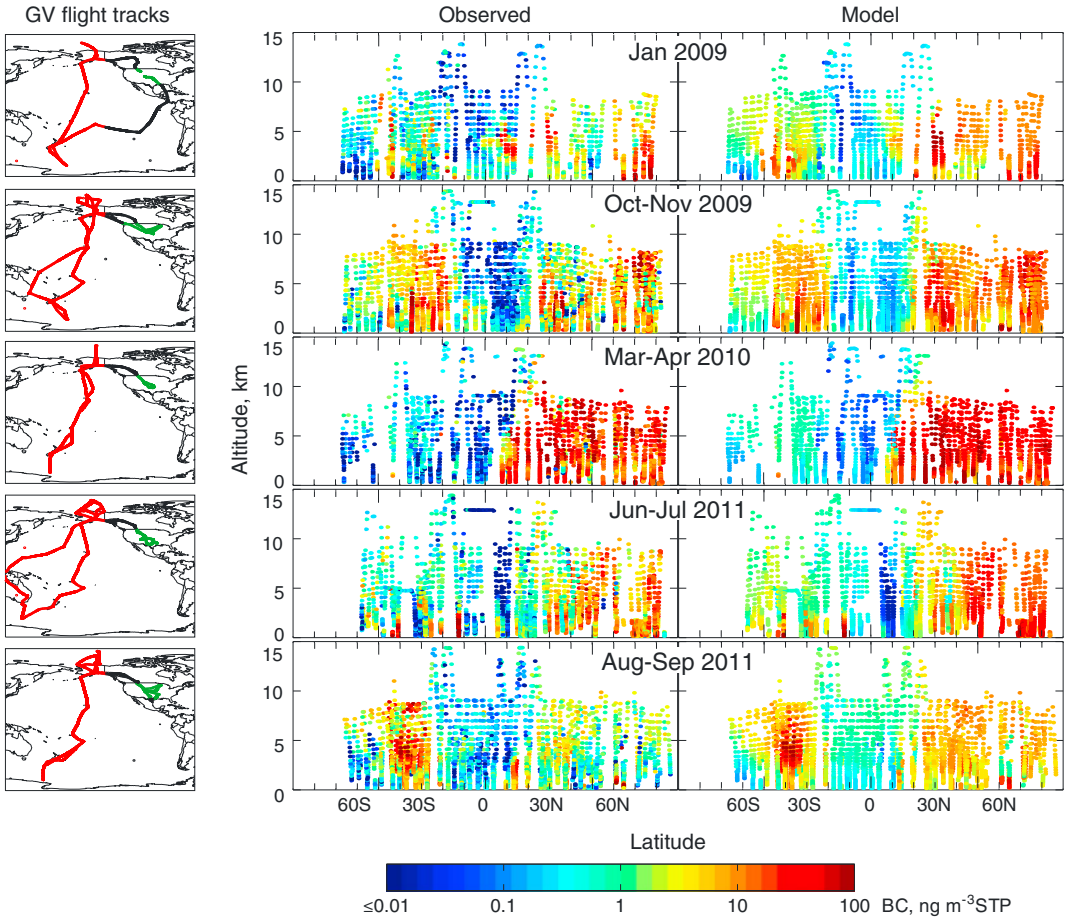

Figure 4. BC concentrations over the central Pacific (west of 140°W) as a function of altitude and latitude for the five HIPPO deployments (red lines on the maps). Observations are compared to GEOS-Chem model results sampled along the flight tracks. Flight tracks over the U.S. (green lines) are not included here but are used for model comparison to observations in Figure 3. Flight tracks over the East Pacific and Canada (black lines) are not used. The observations are averaged over the GEOS-Chem grid and time step of 15 min.

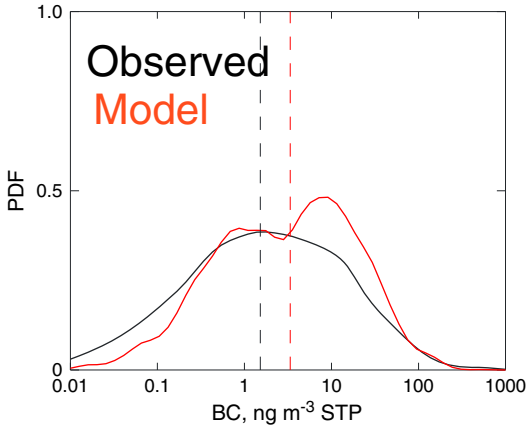

Figure 5. Probability density functions of observed and simulated BC concentrations for the ensemble of HIPPO Central Pacific flight tracks (Figure 4). Dashed lines show the medians.

($[O_3]/[CO] > 1.25$ mol mol^{-1}) [*Hudman et al.*, 2007] and in fire plumes ($[CH_3CN] > 200$ parts per trillion (ppt)) for ARCTAS. All concentrations henceforth are given for standard conditions of temperature and pressure (STP), so that ng m^{-3} STP is a mixing ratio unit.

[20] Figure 3 indicates order-of-magnitude decreases of observed BC concentrations from the boundary layer to the free troposphere over the U.S. and in Asian outflow, reflecting scavenging and dilution during continental ventilation [*Oshima et al.*, 2012]. The model successfully reproduces these decreases. Observations over the Arctic in spring show a mid-troposphere maximum driven by Russian fire effluents and Asian outflow in warm conveyor belts (WCBs) [*Matsui et al.*, 2011]. The model again provides a successful simulation, comparable to that shown in *Wang et al.* [2011] where further analysis of model results for the Arctic is presented. Overall, any biases shown in Figure 3 are relatively small compared to the literature range of model errors for the remote troposphere [*Shindell et al.*, 2008; *Koch et al.*, 2009].

4. BC Distributions Over the Central Pacific

[21] Figure 4 shows latitude-altitude curtains of BC concentrations for the five HIPPO deployments across the Central Pacific. The SP2 instrument detects particles in the 90–600 nm size range, estimated to represent ~90% of total BC mass. An upward correction of 10% is applied to the observations to account for BC mass contained in particles below the SP2 limit of detection [*Schwarz et al.*, 2010]. Observations for individual flights are averaged over the 3-D GEOS-Chem grid, and corresponding model results are sampled along the flight tracks at the same time and location. We focus here on the Central Pacific (Figure 4, red lines) and exclude observations in the stratosphere as diagnosed by $[O_3]/[CO] > 1.25$ mol mol^{-1}.

[22] The SP2 instrument detects individual particles and so its effective detection limit (EDL) varies with collection time and instrument flow rate. The statistical analysis is presented by *Schwarz et al.* [2013]. The EDLs (at the two-sigma level) are 0.01 and 0.1 ng m^{-3} STP for sampling times of 15 min and 1 min respectively near the ground and increase to 0.05 and 0.5 ng m^{-3} STP at 200 hPa. The low concentrations in Figure 4 thus include many individual observations below the EDLs, but the statistical distribution should still be robust. The most prominent feature of the observations in Figure 4 is the strong latitudinal gradient of BC concentrations, with minimum values around the Intertropical Convergence Zone (ITCZ). The model reproduces this feature and attributes the equatorial minimum to scavenging by deep convection. Half of observed concentrations there are below the corresponding EDLs. We see spring maxima of BC concentrations in both the northern and southern extratropics, which the model attributes to efficient continental outflow in the north and to the biomass burning season in the south. Vertical gradients through the troposphere are not systematic and often weak, both in the model and in the observations. Model results are too high in the northern extratropics. More quantitative model evaluation and interpretation is presented below.

[23] Figure 5 shows the probability density function (PDF) of simulated and observed BC concentrations for the ensemble of the data. The observed PDF is approximately lognormal, and this holds also for different HIPPO data subsets. Five percent of observations are below 0.01 ng m^{-3} STP, including 0 values indicating that the SP2 did not see a single BC particle during the integration time. Medians are 1.5 ng m^{-3} STP in the observations and 3.4 ng m^{-3} STP in the model for the ensemble of the data. The bump in the model distribution at 10 ng m^{-3} STP corresponds to the extratropical Northern Hemisphere. Latitudinally binned medians in the observations are 8.3 ng m^{-3} STP at >60°N, 3.1 at 20–60°N, 0.29 at 20°S–20°N, and 1.3 at 20–60°S, all with 30% systematic uncertainty; corresponding model values are 16, 8.8, 0.44, and 2.1 ng m^{-3} STP. The model captures the high end of the observed distribution (>100 ng m^{-3} STP) but not the low end (<0.1 ng m^{-3} STP). Such extremely low observed values, mainly in the tropics (Figure 4), are a remarkable feature of the HIPPO data and must reflect extremely efficient and repeated scavenging that the model cannot reproduce. We find that they are mostly associated with a C_2H_2/CO ratio less than

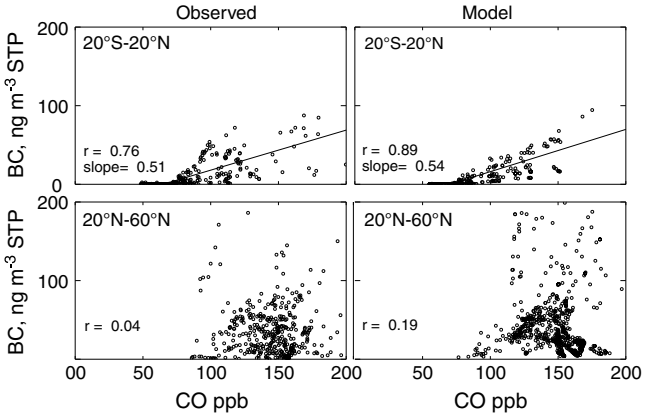

Figure 6. Relationships of BC and CO concentrations in HIPPO from the March–April 2010 deployment in the tropics and northern midlatitudes. Model results (right column) are compared to observations (left column). Correlation coefficients and slopes of reduced-major-axis (RMA) regressions are shown for the tropics.

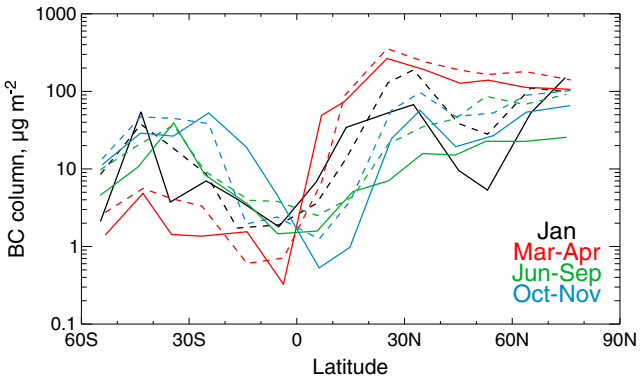

Figure 7. Latitudinal and seasonal variation of BC columns (0–10 km) across the central Pacific during HIPPO for different seasons. The June–September data are for the last two HIPPO deployments (Figure 4). Model results (dashed) are compared to observations (solid).

0.5 ppt ppb^{-1}, indicative of air very remote from combustion influence [*Xiao et al.*, 2007].

[24] We searched for correlations between BC and CO concentrations in the HIPPO data to explain variability in BC concentrations but found these to be in general insignificant due to the dominant role of scavenging in determining BC variability. Fire plumes were the exception. This is illustrated in Figure 6 with scatterplots of observed and model BC versus CO concentrations for 20°S–20°N and 20°–60°N during the March–April 2010 deployment. The tropics show significant correlation in both the model and observations, with consistent slopes, reflecting transport of fire effluents from South Asia. By contrast, there is no correlation at northern midlatitudes, either in the observations or the model.

[25] Figure 7 compares simulated and observed BC columns as a function of latitude for different seasons. The columns were computed by integrating vertical profiles from the surface to 10 km in 10° latitude bands. The latitudinal structure was previously discussed in the context of Figure 4. Maximum and minimum columns span 3 orders of magnitude. Northern Hemisphere columns are highest in March–April when Asian outflow is strongest [*Liu et al.*, 2003]. That is also the period when Southern Hemisphere columns are lowest (wet season in southern tropics). The model reproduces the observed latitudinal and seasonal variation in Figure 7 with $r = 0.92$ and a mean positive bias of 48%. The column bias is relatively smaller than the bias in median concentrations (Figure 5) because the columns are weighted more by high concentrations where the model performs better. Note that radiative forcing due to BC does not scale linearly with columns because of the vertical dependence of radiative forcing efficiency [*Samset and Myhre*, 2011; *Samset et al.*, 2013].

[26] Figure 8 shows median vertical profiles of observed and model BC concentrations for different latitudes and seasons. In the Arctic, BC concentrations tend to increase with altitude in spring and fall, reflecting WCB transport from midlatitudes, but peak near the surface in winter when transport from midlatitudes takes place at low altitudes. At northern and southern midlatitudes, peak concentrations are generally in the free troposphere because of WCB lifting. Tropical concentrations are generally highest near the surface because of scavenging by deep convection. The model fails to reproduce the steep vertical gradient observed in the tropics, suggestive of insufficient scavenging.

[27] We find that the overall high model bias in simulating the HIPPO BC data cannot be readily corrected. It is not due to sources or transport, as discussed above, and presumably reflects errors in scavenging. Our assumption of a fixed 1 day time scale for conversion from hydrophobic to hydrophilic BC is obviously simplistic, and more detailed model treatments have been proposed [*Liu et al.*, 2005; *Stier et al.*, 2005], but one would expect largest sensitivity to this assumption in continental outflow where the model performs well (Figure 3). Assuming BC to be hydrophilic at emission does not actually have much effect in the simulation of continental outflow [*Park et al.*, 2005], and we further reduce this effect in our simulation by scavenging hydrophobic BC by impaction in convective updrafts (see section 2.1).

[28] We can increase the scavenging efficiency in the model by adjustment of other parameters but there is no simple adjustment that improves the ensemble of the HIPPO data, as described in the supporting information, and that does not also compromise other aspects of the model aerosol simulation. It is possible that the model underestimates the frequency of precipitation events in the free troposphere, which would cumulatively affect model results in very remote air. This would be an issue with the GEOS-5 precipitation fields rather than the scavenging parameterization. In any case, our model performs much better in simulating the HIPPO BC data than the ensemble of AeroCom models [*Schwarz et al.*, 2010; *Schwarz et al.*, 2013]. Combined with our successful simulation of BC in source regions and continental outflow (section 3), this provides a basis to use the model for BC source attribution and radiative forcing estimates.

5. Global BC Distribution and Source Attribution

[29] Figure 9 shows the zonal annual mean distribution of BC in GEOS-Chem and the contributions from different

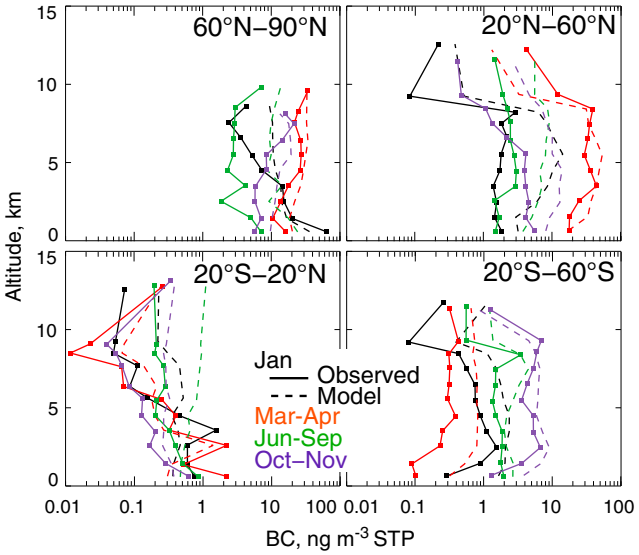

Figure 8. Median profiles of observed and model BC concentrations in different latitude bands and seasons across the central Pacific along HIPPO flight tracks.

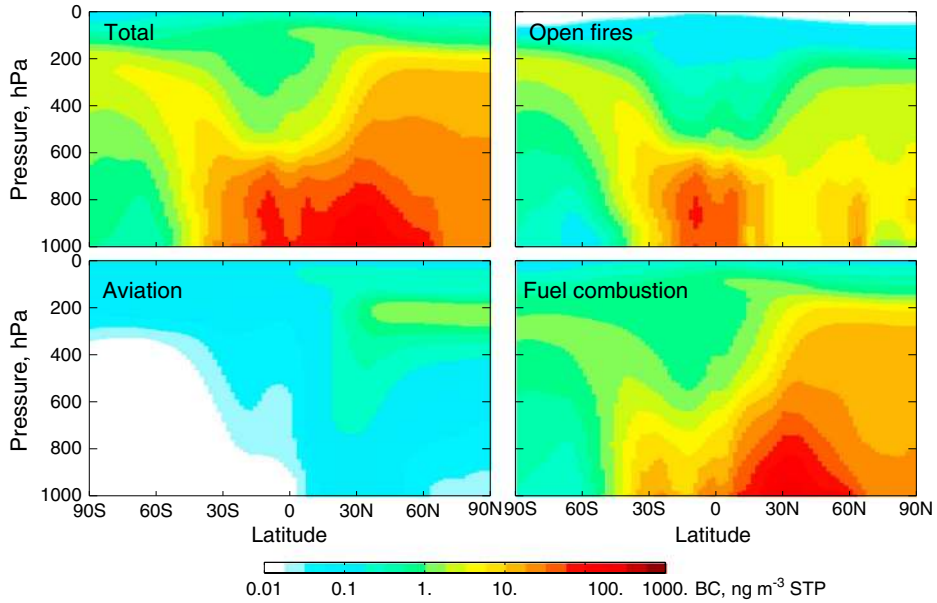

Figure 9. Annual zonal mean concentrations of BC simulated by GEOS-Chem for 2009 as a function of latitude and pressure, with contributions from different source types.

sources in 2009. The ITCZ minimum along the HIPPO flight tracks is not seen in the zonal mean due to the influence of tropical continents. Minima in the zonal mean are instead at high southern latitudes and in the tropical upper troposphere. Fuel combustion dominates in the Northern Hemisphere while open fires are more important in the Southern Hemisphere. Aircraft are important only in the northern stratosphere. We find BC concentrations of 0.4–6 ng m^{-3} STP at 200–100 hPa, consistent with HIPPO observations in the stratosphere [*Schwarz et al*., 2013].

[30] We compute in the model a global atmospheric BC burden of 77 Gg for 2009, of which 0.9 Gg is in the stratosphere. Open fires contribute 31% of the tropospheric burden. The tropospheric lifetime of BC against deposition is 4.2 days. Wet deposition accounts for 77% of the global sink (the rest is from dry deposition), and this is within the range of 63%–94% in previous studies [*Koch*, 2001; *Liu et al*., 2005; *Stier et al*., 2005; *Jacobson*, 2012]. Our lifetime is shorter than the range of 4.9–11.4 days in the AeroCom models [*Schulz et al*., 2006; *Koch et al*., 2009], consistent with our better performance in the simulation of HIPPO and other remote data. The global lifetime of BC is closely related to the efficiency of transport to the free troposphere, where the lifetime is long because of infrequent precipitation. We find in GEOS-Chem that 33% of the BC burden is in the free troposphere above 2 km and 8.7% is above 5 km. In comparison, the AeroCom models have 21 ± 11% of BC above 5 km [*Schulz et al*., 2006]. This has important implications for radiative forcing because BC in the free troposphere is more likely to be above clouds and thus has a large radiative forcing efficiency [*Samset and Myhre*, 2011; *Samset et al*., 2013].

6. Global BC AAOD and Radiative Forcing

[31] Figure 10 shows the global annual mean distribution of BC AAOD (here and after, AAOD is for a wavelength of 550 nm) in the model and compares with observations from the AERONET. We compute the AAOD in the model as a product of the BC column and a constant mass absorption coefficient (MAC) of 11.3 m^2 g^{-1} based on atmospheric observations and thus accounting for appropriate mean mixing with other aerosol types [*Bond and Bergstrom*, 2006]. The model results are for 2009. The observed BC AAODs are 1996–2011 averages from AERONET level 2.0 data together with level 1.5 data for low-AOD conditions so as to minimize sampling bias (ftp://ftp-projects.zmaw.de/aerocom/aeronet/STATISTICS/grd_1203/). BC AAOD is retrieved by applying the refractive index for total aerosol to fine-mode aerosol (particles with diameter < 1 μm) and assuming all fine-mode AAOD to be from BC.

[32] The model gives a global mean BC AAOD of 0.0017. Comparison to the AERONET sites in Figure 10 indicates a

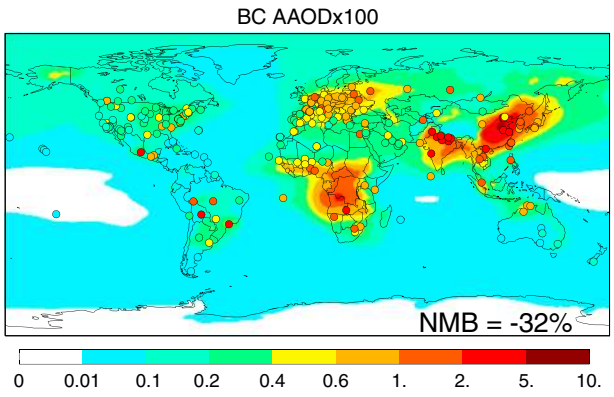

Figure 10. Global distribution of BC absorbing aerosol optical depth (AAOD) at 550 nm. Annual mean model values for 2009 (background) are compared to AERONET observations for 1996–2011 (circles). The AERONET data were obtained from ftp://ftp-projects.zmaw.de/aerocom/aeronet/STATISTICS/grd_1203/.

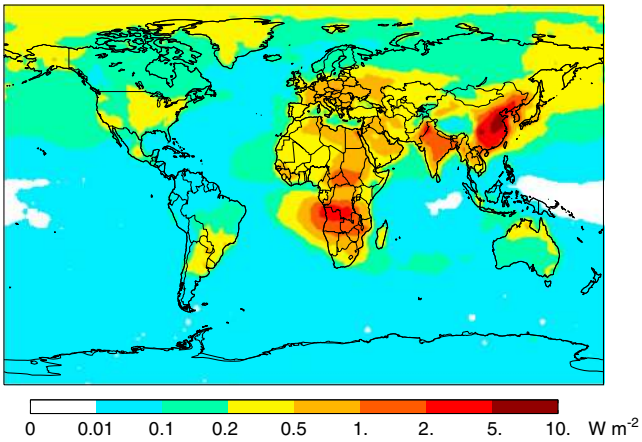

Figure 11. Global annual mean distribution of BC direct radiative forcing (DRF) at the top of the atmosphere (TOA). The radiative transfer model of *Wang et al*. [2008, 2013] is applied to the 3-D distribution of BC mass concentrations from GEOS-Chem.

global normalized mean bias (NMB) of −32% relative to the AERONET data. The bias is less in extratropical northern latitudes (−22%) than in the tropics (−65%). Part of the tropical bias could reflect interannual variability of fires, as GFED3 BC emissions from fires are 1.6 Tg a^{-1} for 2009 but 2.1 ± 0.40 Tg a^{-1} for the 1996–2011 average. The NMB in the topics would decrease to −50% with model results for 2010 (open fire emissions of 2.3 Tg a^{-1}). *Randerson et al*. [2012] argued that the GFED3 inventory is globally too low by 26% because it underestimates small fires.

[33] The oceans account for 41% of global BC AAOD in the model. The AERONET data are almost exclusively over continents, but there are a few island sites (Figure 10). Comparison to these sites shows a high model bias over the northern Pacific, consistent with HIPPO, but a low bias over the tropical oceans, which is inconsistent with HIPPO.

[34] There are large uncertainties associated with the AERONET BC AAOD data. *Bond et al*. [2013] argued that values should be increased by 75% through better coarse-mode refractive index assumptions. On the other hand, *Chung et al*. [2012] argued that organic carbon (OC) aerosol accounts for 20% of fine-mode absorption. Combining factors in these two studies would imply a multiplicative factor of 1.4 (1.75 × 0.8) to the AERONET data in Figure 10 and a model NMB of −51% (a factor of 2). AERONET observes only under clear skies but comparison of clear-sky to all-sky conditions in our model suggests that the resulting bias is insignificant (3%), consistent with the results of *Bond et al*. [2013].

[35] Figure 11 shows the global distribution of annual TOA DRF based on 3-D fields of BC concentrations with 6 h resolution for the year 2009 in GEOS-Chem. The global mean TOA DRF is 0.19 W m^{-2}. The forcing calculation follows *Wang et al*. [2008] but with improvement in the treatment of cloud effects [*Wang et al*., 2013]. The cloud data are from GEOS-5 with 6 h resolution; global mean cloud cover is 58%, consistent with a best estimate of 65% from the International Satellite Cloud Climatology Project (http://isccp.giss.nasa.gov/climanal1.html). A four-stream broadband radiative transfer model (RTM), using monthly mean surface reflectance data [*Koelemeijer et al*., 2003], is employed for the forcing calculation. The RTM is applied to the solar spectrum for six bands ranging from 0.2 to 4 μm. It assumes that BC particles are spherical with a refractive index at 550 nm of 1.76 + 0.47*i* and a density of 1 g cm^{-3}. The low refractive imaginary index (compared to that of the void fraction line in the work of *Bond and Bergstrom* [2006]) would underestimate MAC, while the low density (compared to 1.7–1.9 g cm^{-3} suggested by *Bond and Bergstrom* [2006]) would overestimate it. Therefore, the derived MAC for BC of 11.3 m^2 g^{-1} at 550 nm (consistent with our AAOD calculation) is comparable to the MAC recommended by *Bond and Bergstrom* [2006] and *Bond et al*. [2013].

[36] The global distribution of TOA DRF generally follows the AAOD pattern in Figure 10 but with elevated forcing in polar regions. This reflects higher aerosol forcing efficiency (AFE, defined as the TOA DRF normalized by BC AAOD) associated with high surface albedo and high solar zenith angle [*Samset and Myhre*, 2011]. The oceans

Table 2. Top-of-Atmosphere BC Direct Radiative Forcing (DRF) and Driving Variables[a]

Reference	Emission (Tg a^{-1})	Lifetime (d)	Load (mg m^{-2})	Load above 5 km (%)	MAC (m^2 g^{-1})	AAOD ×100	AFE (W m^{-2}/AAOD)	DRF (W m^{-2})
This work[b]	6.5	4.2	0.15	8.7	11	0.17(0.14–0.26)	114	0.19(0.17–0.31)
Jacobson [2000]			0.45					0.54
Schulz et al. [2006][c]	6.3	6.8 ± 1.8	0.23 ± 0.07	21 ± 11	7.9 ± 1.9	0.18 ± 0.08	168 ± 53	0.27 ± 0.06
Ramanathan and Carmichael [2008][d]						0.67	134	0.9
Chung et al. [2012][e]						0.77	84	0.65
Jacobson [2012][f]	9.3	3.2	0.18		16	0.28		
Bond et al. [2013][g]	17	6.1	0.55		11	0.60	147	0.88

[a]Global results for BC from all sources. Lifetime is tropospheric lifetime against deposition, estimated as the ratio of the column burden to the total source, MAC is the mass absorption coefficient, and AFE is the aerosol forcing efficiency.
[b]Ranges given for AAOD and DRF reflect model adjustments to match either the HIPPO or AERONET data (see text).
[c]Averages and standard deviations for eight models from AeroCom Phase I simulations (the ULAQ model is not included as it only reports clear-sky forcing). All AeroCom models use the same emissions. Results from AeroCom Phase II simulations [*Myhre et al*., 2013] are not presented here because they report BC forcings from fuel sources only.
[d]AAODs derived from a combination of AERONET observations, MODIS satellite observations, and the GOCART model.
[e]AAODs derived from a combination of AERONET observations, MODIS and MISR satellite observations, and the GOCART model.
[f]Simulation focused on cloud absorption effects and did not provide DRF.
[g]From AeroCom Phase I simulations with scaling factors to match AERONET AAODs.

account for 41% of the global AAOD and 36% of the TOA DRF. The AFE tends to be lower than average over the oceans because the surface is dark.

[37] We can estimate the uncertainty in our TOA DRF estimate associated with the global BC distribution. The model shows little bias relative to in situ observations in source regions and continental outflow. It is however too high relative to the HIPPO data (+48% column mean bias) and too low relative to the AERONET AAOD data (possibly a factor of 2 as discussed above). We cannot reconcile these opposite biases with our model. If we discount the AERONET data and decrease the model AAOD over the oceans by 32% to correct the HIPPO overestimate, we obtain as lower bound a global BC AAOD of 0.0014 and TOA DRF of 0.17 W m^{-2}. If we discount the in situ continental data and increase the model AAOD over land by a factor of 2 to match the AERONET data with corrections from *Bond et al*. [2013] and *Chung et al*. [2012], we obtain as upper bound a global BC AAOD of 0.0026 and TOA DRF of 0.31 W m^{-2}. There are additional uncertainties related to the mixing state of BC and the radiative transfer model. Comparisons to previous studies are presented in the next section.

7. Comparison With Previous Studies

[38] Previous studies of BC radiative forcing have used various models to simulate the global distribution of BC, sometimes in combination with constraints from AERONET and satellite observations. Table 2 compiles results from recent studies and from the AeroCom activity Phase I [*Schulz et al*., 2006], which intercompared results from eight models. AeroCom Phase II [*Myhre et al*., 2013] has results similar to Phase I but only reports forcing for fuel BC (not including open fires) and so is not included in the table.

[39] We see from Table 2 that our best estimate of 0.19 W m^{-2} for BC radiative forcing is below the range of previous studies. To understand the differences, we can express the DRF as the product of four driving variables [*Bond et al*., 2013]:

$$\mathrm{DRF} = \mathrm{Emission} \times \mathrm{Lifetime} \times \mathrm{MAC} \times \mathrm{AFE} \quad (2)$$

[40] Our global emission of BC (6.5 Tg a^{-1}) is similar to the AeroCom value of 6.3 Tg a^{-1}, 30% lower than the *Jacobson* [2012] value, and much lower than the *Bond et al*. [2013] value of 17 Tg a^{-1} which was scaled to match AERONET AAOD observations. An emission of 17 Tg a^{-1} cannot be reconciled with the ensemble of in situ observations presented here, at least in the context of GEOS-Chem. It would produce a large positive bias in source regions, in continental outflow, and in the HIPPO data. Correcting for this bias would require a very short BC lifetime (less than 3 days).

[41] We compute a global tropospheric lifetime of 4.2 days for BC in GEOS-Chem, much lower than 6.8 ± 1.8 days in AeroCom and 6.1 days in *Bond et al*. [2013]. This reflects our modifications to the GEOS-Chem wet scavenging scheme to better match the HIPPO observations while retaining consistency with other observations. Prior to these modifications, the tropospheric lifetime of BC in GEOS-Chem was 5.9 days [*Wang et al*., 2011]. The longer lifetime in the AeroCom models is likely responsible for their order-of-magnitude overestimates of the HIPPO data [*Schwarz et al*., 2010; *Schwarz et al*., 2013]. This has important implications because a longer BC lifetime allows for a greater load at high altitude where the BC radiative forcing efficiency is high. *Jacobson* [2012] gave even shorter lifetime of 3.2 days and reproduced HIPPO observations in January 2009, although the comparison was conducted for the whole data set and was weighted toward source regions, including U.S. and Central America (see flight tracks in Figure 4).

[42] We obtain an atmospheric load for BC of 0.15 mg m^{-2} (77 Gg), consistent with the *Jacobson* [2012] value of 0.18 mg m^{-2} but much lower than the AeroCom value of 0.23 ± 0.07 mg m^{-2}, the *Jacobson* [2000] value of 0.45 mg m^{-2}, or the *Bond et al*. [2013] value of 0.55 mg m^{-2}. Our estimate of the atmospheric load is most consistent with the ensemble of in situ observations presented in this paper. It underestimates the AERONET observations by as much as a factor 2 but there is large uncertainty in these observations as discussed above. The AERONET data provide little information over the oceans and no information on the vertical distribution of BC, which is critical for the DRF calculation. The fraction of the global BC load residing above 5 km is 8.7% in GEOS-Chem but 21 ± 11% in the AeroCom models for Phase I [*Schulz et al*., 2006] and 23 ± 11% for Phases I and II [*Samset et al*., 2013]. The contribution to global DRF from BC above 5 km is 13% in GEOS-Chem but 41 ± 14% in *Samset et al*. [2013].

[43] Our global BC AAOD estimate (0.0017) is consistent with AeroCom (0.0018 ± 0.0008) but this reflects their assumption of a small MAC (7.9 m^2 g^{-1}). It is now considered that 11 m^2 g^{-1} (as used in our work) is more appropriate [*Bond and Bergstrom*, 2006; *Bond et al*., 2013]. *Jacobson* [2012] found an even larger MAC (16 m^2 g^{-1}) by accounting for conditions of high relative humidity (RH) and inferred from there a BC AAOD of 0.0028. Applying MAC of 16 m^2 g^{-1} in our study would reduce our model bias compared with AERONET BC AAOD, and result in an AAOD of 0.0024 and DRF of 0.27 W m^{-2}. However, accounting for high-RH environments is very uncertain in global models because of subgrid variability and related cloud formation [*Adams et al*., 2001]. Other studies in Table 2 give much higher values for BC AAOD (0.0060–0.0077), reflecting their use of AERONET constraints over land but also excessive BC concentrations over the oceans that would vastly overestimate the HIPPO data.

[44] Our AFE of 114 W m^{-2} reflects application of the *Wang et al*. [2008, 2013] RTM to our global 3-D BC concentration fields. It is higher than the value of *Chung et al*. [2012] (84 W m^{-2}) but lower than other reported values in Table 2 (134–168 W m^{-2}). Differences in AFE may reflect in part differences in model clouds and aerosol optical properties, but also the vertical distribution of BC [*Samset et al*., 2013; *Stier et al*., 2013]. Our lower AFE relative to AeroCom is consistent with our lower fraction of BC in the upper troposphere, supported by the aircraft data.

8. Conclusions

[45] We used the GOES-Chem chemical transport model (CTM) to interpret extensive vertical profiles of black carbon (BC) concentrations from the HIPPO campaign in five deployments across the central Pacific from 85°N to 67°S during 2009–2011. Our goal was to better understand the

factors controlling BC concentrations in the remote troposphere and the implications for BC radiative forcing.

[46] The HIPPO observations indicate very low BC concentrations over the Pacific, particularly in the tropics where values are often less than 0.1 ng m^{-3} STP through the depth of the troposphere. Reproducing these observations requires more efficient wet scavenging of BC than is usually implemented in models. We find that a GEOS-Chem simulation with global BC source of 6.5 Tg a^{-1}, and an improved representation of scavenging leading to a tropospheric BC lifetime of 4.2 days, reproduces the general features of the HIPPO data although it is biased high by a factor of 2 in median concentrations and 1.48 in column load. It also provides a successful simulation of BC concentrations in northern midlatitudes source regions and continental outflow. Comparison to global AERONET absorbing aerosol optical depth (AAOD) data indicates a mean underestimate of 32%, although the magnitude of this bias depends on the assumptions in the AERONET product.

[47] It appears from the HIPPO data that BC concentrations over the remote oceans, and in particular in the upper troposphere, are considerably lower than in the AeroCom CTMs commonly used for BC radiative forcing estimates. Reproducing these low concentrations in GEOS-Chem required an increase in the efficiency of BC scavenging, consistent with findings in other model studies [*Jacobson*, 2012; *Kipling et al*., 2013]. Longer BC lifetimes in the AeroCom models (6.8 ± 1.8 days) allow more BC to reach the free troposphere where its radiation forcing efficiency is larger. We find in GEOS-Chem that 8.7% of the BC load is in the free troposphere above 5 km, compared to $21 \pm 11\%$ in the AeroCom models.

[48] We combined our global 3-D distribution of BC concentrations with a radiative transfer model to infer a global top-of-atmosphere DRF for BC of 0.19 W m^{-2}, with an uncertainty range of 0.17 - 0.31 W m^{-2} based on uncertainty in the BC atmospheric distribution. This is lower than the estimate of 0.27 ± 0.06 W m^{-2} from the AeroCom models [*Schulz et al*., 2006] and much lower than more recent estimates of 0.65–0.9 W m^{-2} [*Chung et al*., 2012; *Bond et al*., 2013]. We find that the difference is largely driven by the estimates of BC concentrations over the oceans and in the free troposphere. Based on the constraints offered by the HIPPO observations and consistent also with other BC data, it appears that the radiative forcing from BC is less than previously thought.

[49] **Acknowledgment.** This work was supported by the U.S. National Science Foundation.

References

Adams, P. J., J. H. Seinfeld, D. Koch, L. Mickley, and D. Jacob (2001), General circulation model assessment of direct radiative forcing by the sulfate-nitrate-ammonium-water inorganic aerosol system, *J. Geophys. Res.*, *106*(D1), 1097–1111, doi:10.1029/2000JD900512.

Balkanski, Y. J., D. J. Jacob, G. M. Gardner, W. C. Graustein, and K. K. Turekian (1993), Transport and residence times of tropospheric aerosols inferred from a global three-dimensional simulation of ^{210}Pb, *J. Geophys. Res.*, *98*(D11), 20,573–20,586, doi:10.1029/93JD02456.

Bond, T. C., and R. W. Bergstrom (2006), Light absorption by carbonaceous particles: An investigative review, *Aerosol Sci. Technol.*, *40*(1), 27–67, doi:10.1080/02786820500421521.

Bond, T. C., E. Bhardwaj, R. Dong, R. Jogani, S. K. Jung, C. Roden, D. G. Streets, and N. M. Trautmann (2007), Historical emissions of black and organic carbon aerosol from energy-related combustion, 1850–2000, *Global Biogeochem. Cycles*, *21*, Gb2018, doi:10.1029/2006GB002840.

Bond, T. C., et al. (2013), Bounding the role of black carbon in the climate system: A scientific assessment, *J. Geophys. Res. Atmos.*, *118*, 5380–5552, doi:10.1002/jgrd.50171.

Chung, C. E., V. Ramanathan, D. Kim, and I. A. Podgorny (2005), Global anthropogenic aerosol direct forcing derived from satellite and ground-based observations, *J. Geophys. Res.*, *110*(D24), D24207, doi:10.1029/2005JD006356.

Chung, C. E., V. Ramanathan, and D. Decremer (2012), Observationally constrained estimates of carbonaceous aerosol radiative forcing, *Proc. Natl. Acad. Sci. U.S.A.*, *109*(29), 11,624–11,629, doi:10.1073/pnas.1203707109.

Cooke, W. F., C. Liousse, H. Cachier, and J. Feichter (1999), Construction of a 1 degrees × 1 degrees fossil fuel emission data set for carbonaceous aerosol and implementation and radiative impact in the ECHAM4 model, *J. Geophys. Res.*, *104*(D18), 22,137–22,162.

Croft, B., U. Lohmann, R. V. Martin, P. Stier, S. Wurzler, J. Feichter, C. Hoose, U. Heikkila, A. van Donkelaar, and S. Ferrachat (2010), Influences of in-cloud aerosol scavenging parameterizations on aerosol concentrations and wet deposition in ECHAM5-HAM, *Atmos. Chem. Phys.*, *10*(4), 1511–1543.

Drury, E., D. J. Jacob, R. J. D. Spurr, J. Wang, Y. Shinozuka, B. E. Anderson, A. D. Clarke, J. Dibb, C. McNaughton, and R. Weber (2010), Synthesis of satellite (MODIS), aircraft (ICARTT), and surface (IMPROVE, EPA-AQS, AERONET) aerosol observations over eastern North America to improve MODIS aerosol retrievals and constrain surface aerosol concentrations and sources, *J. Geophys. Res.*, *115*, D14204, doi:10.1029/2009JD012629.

Dubovik, O., B. Holben, T. F. Eck, A. Smirnov, Y. J. Kaufman, M. D. King, D. Tanre, and I. Slutsker (2002), Variability of absorption and optical properties of key aerosol types observed in worldwide locations, *J. Atmos. Sci.*, *59*(3), 590–608, doi:10.1175/1520-0469(2002)059<0590:voaaop>2.0.co;2.

Ekman, A. M. L., C. Wang, J. Wilson, and J. Strom (2004), Explicit simulations of aerosol physics in a cloud-resolving model: A sensitivity study based on an observed convective cloud, *Atmos. Chem. Phys.*, *4*, 773–791.

Flanner, M. G., C. S. Zender, J. T. Randerson, and P. J. Rasch (2007), Present-day climate forcing and response from black carbon in snow, *J. Geophys. Res.*, *112*, D11202, doi:10.1029/2006JD008003.

Fornea, A. P., S. D. Brooks, J. B. Dooley, and A. Saha (2009), Heterogeneous freezing of ice on atmospheric aerosols containing ash, soot, and soil, *J. Geophys. Res.*, *114*, D13201, doi:10.1029/2009JD011958.

Friedman, B., G. Kulkarni, J. Beranek, A. Zelenyuk, J. A. Thornton, and D. J. Cziczo (2011), Ice nucleation and droplet formation by bare and coated soot particles, *J. Geophys. Res.*, *116*, D17203, doi:10.1029/2011JD015999.

Fu, T. M., et al. (2012), Carbonaceous aerosols in China: Top-down constraints on primary sources and estimation of secondary contribution, *Atmos. Chem. Phys.*, *12*(5), 2725–2746, doi:10.5194/acp-12-2725-2012.

Gorbunov, B., A. Baklanov, N. Kakutkina, H. L. Windsor, and R. Toumi (2001), Ice nucleation on soot particles, *J. Aerosol Sci.*, *32*(2), 199–215, doi:10.1016/s0021-8502(00)00077-x.

Huang, L., S. L. Gong, C. Q. Jia, and D. Lavoue (2010), Importance of deposition processes in simulating the seasonality of the Arctic black carbon aerosol, *J. Geophys. Res.*, *115*, D17207, doi:10.1029/2009JD013478.

Hudman, R. C., et al. (2007), Surface and lightning sources of nitrogen oxides over the United States: Magnitudes, chemical evolution, and outflow, *J. Geophys. Res.*, *112*, D12s05, doi:10.1029/2006JD007912.

Jacob, D. J., et al. (1997), Evaluation and intercomparison of global atmospheric transport models using ^{222}Rn and other short-lived tracers, *J. Geophys. Res.*, *102*(D5), 5953–5970, doi:10.1029/96JD02955.

Jacob, D. J., et al. (2010), The Arctic Research of the Composition of the Troposphere from Aircraft and Satellites (ARCTAS) mission: Design, execution, and first results, *Atmos. Chem. Phys.*, *10*(11), 5191–5212, doi:10.5194/acp-10-5191-2010.

Jacobson, M. Z. (2000), A physically-based treatment of elemental carbon optics: Implications for global direct forcing of aerosols, *Geophys. Res. Lett.*, *27*(2), 217–220, doi:10.1029/1999GL010968.

Jacobson, M. Z. (2001), Strong radiative heating due to the mixing state of black carbon in atmospheric aerosols, *Nature*, *409*(6821), 695–697.

Jacobson, M. Z. (2012), Investigating cloud absorption effects: Global absorption properties of black carbon, tar balls, and soil dust in clouds and aerosols, *J. Geophys. Res.*, *117*, D06205, doi:10.1029/2011JD017218.

Kipling, Z., P. Stier, J. P. Schwarz, A. E. Perring, J. R. Spackman, G. W. Mann, C. E. Johnson, and P. J. Telford (2013), Constraints on aerosol processes in climate models from vertically-resolved aircraft observations of black carbon, *Atmos. Chem. Phys.*, *13*(12), 5969–5986, doi:10.5194/acp-13-5969-2013.

Koch, D. (2001), Transport and direct radiative forcing of carbonaceous and sulfate aerosols in the GISS GCM, *J. Geophys. Res.*, *106*(D17), 20,311–20,332, doi:10.1029/2001JD900038.

Koch, D., T. C. Bond, D. Streets, N. Unger, and G. R. van der Werf (2007), Global impacts of aerosols from particular source regions and sectors, *J. Geophys. Res.*, *112*, D02205, doi:10.1029/2005JD007024.

Koch, D., et al. (2009), Evaluation of black carbon estimations in global aerosol models, *Atmos. Chem. Phys.*, *9*(22), 9001–9026.

Koehler, K. A., P. J. DeMott, S. M. Kreidenweis, O. B. Popovicheva, M. D. Petters, C. M. Carrico, E. D. Kireeva, T. D. Khokhlova, and N. K. Shonija (2009), Cloud condensation nuclei and ice nucleation activity of hydrophobic and hydrophilic soot particles, *Phys. Chem. Chem. Phys.*, *11*(36), 7906–7920, doi:10.1039/b905334b.

Koelemeijer, R. B. A., J. F. de Haan, and P. Stammes (2003), A database of spectral surface reflectivity in the range 335–772 nm derived from 5.5 years of GOME observations, *J. Geophys. Res.*, *108*(D2), 4070, doi:10.1029/2002JD002429.

Leibensperger, E. M., L. J. Mickley, D. J. Jacob, W. T. Chen, J. H. Seinfeld, A. Nenes, P. J. Adams, D. G. Streets, N. Kumar, and D. Rind (2012), Climatic effects of 1950–2050 changes in US anthropogenic aerosols—Part 1: Aerosol trends and radiative forcing, *Atmos. Chem. Phys.*, *12*(7), 3333–3348, doi:10.5194/acp-12-3333-2012.

Liu, H. Y., D. J. Jacob, I. Bey, and R. M. Yantosca (2001), Constraints from Pb-210 and Be-7 on wet deposition and transport in a global three-dimensional chemical tracer model driven by assimilated meteorological fields, *J. Geophys. Res.*, *106*(D11), 12,109–12,128.

Liu, H. Y., D. J. Jacob, I. Bey, R. M. Yantosca, B. N. Duncan, and G. W. Sachse (2003), Transport pathways for Asian pollution outflow over the Pacific: Interannual and seasonal variations, *J. Geophys. Res.*, *108*(D20), 8786, doi:10.1029/2002JD003102.

Liu, X., J. E. Penner, and M. Herzog (2005), Global modeling of aerosol dynamics: Model description, evaluation, and interactions between sulfate and nonsulfate aerosols, *J. Geophys. Res.*, *110*(D18), D18206, doi:10.1029/2004JD005674.

Liu, J. F., S. M. Fan, L. W. Horowitz, and H. Levy (2011), Evaluation of factors controlling long-range transport of black carbon to the Arctic, *J. Geophys. Res.*, *116*, D04307, doi:10.1029/2010JD015145.

Mao, Y. H., Q. B. Li, L. Zhang, Y. Chen, J. T. Randerson, D. Chen, and K. N. Liou (2011), Biomass burning contribution to black carbon in the Western United States Mountain Ranges, *Atmos. Chem. Phys.*, *11*(21), 11,253–11,266, doi:10.5194/acp-11-11253-2011.

Matsui, H., et al. (2011), Seasonal variation of the transport of black carbon aerosol from the Asian continent to the Arctic during the ARCTAS aircraft campaign, *J. Geophys. Res.*, *116*, D05202, doi:10.1029/2010JD015067.

McConnell, J. R., R. Edwards, G. L. Kok, M. G. Flanner, C. S. Zender, E. S. Saltzman, J. R. Banta, D. R. Pasteris, M. M. Carter, and J. D. W. Kahl (2007), 20th-century industrial black carbon emissions altered Arctic climate forcing, *Science*, *317*(5843), 1381–1384, doi:10.1126/science.1144856.

Myhre, G., et al. (2013), Radiative forcing of the direct aerosol effect from AeroCom Phase II simulations, *Atmos. Chem. Phys.*, *13*(4), 1853–1877, doi:10.5194/acp-13-1853-2013.

Oshima, N., et al. (2012), Wet removal of black carbon in Asian outflow: Aerosol Radiative Forcing in East Asia (A-FORCE) aircraft campaign, *J. Geophys. Res.*, *117*, D03204, doi:10.1029/2011JD016552.

Park, R. J., D. J. Jacob, M. Chin, and R. V. Martin (2003), Sources of carbonaceous aerosols over the United States and implications for natural visibility, *J. Geophys. Res.*, *108*(D12), 4355, doi:10.1029/2002JD003190.

Park, R. J., et al. (2005), Export efficiency of black carbon aerosol in continental outflow: Global implications, *J. Geophys. Res.*, *110*, D11205, doi:10.1029/2004JD005432.

Park, R. J., D. J. Jacob, N. Kumar, and R. M. Yantosca (2006), Regional visibility statistics in the United States: Natural and transboundary pollution influences, and implications for the Regional Haze Rule, *Atmos. Environ.*, *40*(28), 5405–5423, doi:10.1016/j.atmosenv.2006.04.059.

Quinn, P. K., et al. (2008), Short-lived pollutants in the Arctic: Their climate impact and possible mitigation strategies, *Atmos. Chem. Phys.*, *8*(6), 1723–1735.

Ramanathan, V., and G. Carmichael (2008), Global and regional climate changes due to black carbon, *Nat. Geosci.*, *1*(4), 221–227, doi:10.1038/ngeo156.

Randerson, J. T., Y. Chen, G. R. van der Werf, B. M. Rogers, and D. C. Morton (2012), Global burned area and biomass burning emissions from small fires, *J. Geophys. Res.*, *117*, G04012, doi:10.1029/2012JG002128.

Rasch, P. J., et al. (2000), A comparison of scavenging and deposition processes in global models: Results from the WCRP Cambridge Workshop of 1995, *Tellus B*, *52*(4), 1025–1056, doi:10.1034/j.1600-0889.2000.00980.x.

Reddy, M. S., and O. Boucher (2004), A study of the global cycle of carbonaceous aerosols in the LMDZT general circulation model, *J. Geophys. Res.*, *109*, D14202, doi:10.1029/2003JD004048.

Remer, L. A., et al. (2005), The MODIS aerosol algorithm, products, and validation, *J. Atmos. Sci.*, *62*(4), 947–973, doi:10.1175/jas3385.1.

Riemer, N., M. West, R. Zaveri, and R. Easter (2010), Estimating black carbon aging time-scales with a particle-resolved aerosol model, *J. Aerosol Sci.*, *41*(1), 143–158, doi:10.1016/j.jaerosci.2009.08.009.

Samset, B. H., and G. Myhre (2011), Vertical dependence of black carbon, sulphate and biomass burning aerosol radiative forcing, *Geophys. Res. Lett.*, *38*, L24802, doi:10.1029/2011GL049697.

Samset, B. H., et al. (2013), Black carbon vertical profiles strongly affect its radiative forcing uncertainty, *Atmos. Chem. Phys.*, *13*(5), 2423–2434, doi:10.5194/acp-13-2423-2013.

Sato, M., J. Hansen, D. Koch, A. Lacis, R. Ruedy, O. Dubovik, B. Holben, M. Chin, and T. Novakov (2003), Global atmospheric black carbon inferred from AERONET, *Proc. Natl. Acad. Sci. U.S.A.*, *100*(11), 6319–6324, doi:10.1073/pnas.0731897100.

Schulz, M., et al. (2006), Radiative forcing by aerosols as derived from the AeroCom present-day and pre-industrial simulations, *Atmos. Chem. Phys.*, *6*, 5225–5246.

Schwarz, J. P., J. R. Spackman, R. S. Gao, L. A. Watts, P. Stier, M. Schulz, S. M. Davis, S. C. Wofsy, and D. W. Fahey (2010), Global-scale black carbon profiles observed in the remote atmosphere and compared to models, *Geophys. Res. Lett.*, *37*, L18812, doi:10.1029/2010GL044372.

Schwarz, J. P., B. H. Samset, A. E. Perring, J. R. Spackman, R. S. Gao, P. Stier, M. Schulz, F. L. Moore, E. A. Ray, and D. W. Fahey (2013), Global-scale seasonally resolved black carbon vertical profiles over the Pacific, *Geophys. Res. Lett.*, *40*, 5542–5547, doi:10.1002/2013GL057775.

Shindell, D. T., et al. (2008), A multi-model assessment of pollution transport to the Arctic, *Atmos. Chem. Phys.*, *8*(17), 5353–5372.

Simone, N. W., M. E. J. Stettler, and S. R. H. Barrett (2013), Rapid estimation of global civil aviation emissions with uncertainty quantification, *Transport. Res. Part D*, *25*, 33–41, doi:10.1016/j.trd.2013.07.001.

Stier, P., et al. (2005), The aerosol-climate model ECHAM5-HAM, *Atmos. Chem. Phys.*, *5*(4), 1125–1156, doi:10.5194/acp-5-1125-2005.

Stier, P., et al. (2013), Host model uncertainties in aerosol radiative forcing estimates: Results from the AeroCom prescribed intercomparison study, *Atmos. Chem. Phys.*, *13*(6), 3245–3270, doi:10.5194/acp-13-3245-2013.

Torres, O., A. Tanskanen, B. Veihelmann, C. Ahn, R. Braak, P. K. Bhartia, P. Veefkind, and P. Levelt (2007), Aerosols and surface UV products from Ozone Monitoring Instrument observations: An overview, *J. Geophys. Res.*, *112*, D24s47, doi:10.1029/2007JD008809.

Wang, Y., D. J. Jacob, and J. A. Logan (1998), Global simulation of tropospheric O_3-NO_x-hydrocarbon chemistry—1. Model formulation, *J. Geophys. Res.*, *103*(D9), 10,713–10,725, doi:10.1029/98JD00158.

Wang, J., D. J. Jacob, and S. T. Martin (2008), Sensitivity of sulfate direct climate forcing to the hysteresis of particle phase transitions, *J. Geophys. Res.*, *113*, D11207, doi:10.1029/2007JD009368.

Wang, Q., et al. (2011), Sources of carbonaceous aerosols and deposited black carbon in the Arctic in winter-spring: Implications for radiative forcing, *Atmos. Chem. Phys.*, *11*(23), 12,453–12,473, doi:10.5194/acp-11-12453-2011.

Wang, J., S. Park, J. Zeng, C. Ge, K. Yang, S. Carn, N. Krotkov, and A. H. Omar (2013), Modeling of 2008 Kasatochi volcanic sulfate direct radiative forcing: Assimilation of OMI SO2 plume height data and comparison with MODIS and CALIOP observations, *Atmos. Chem. Phys.*, *13*(4), 1895–1912, doi:10.5194/acp-13-1895-2013.

Warren, S. G., and W. J. Wiscombe (1985), Dirty snow after nuclear-war, *Nature*, *313*(6002), 467–470.

van der Werf, G. R., J. T. Randerson, L. Giglio, G. J. Collatz, M. Mu, P. S. Kasibhatla, D. C. Morton, R. S. DeFries, Y. Jin, and T. T. van Leeuwen (2010), Global fire emissions and the contribution of deforestation, savanna, forest, agricultural, and peat fires (1997–2009), *Atmos. Chem. Phys.*, *10*(23), 11,707–11,735, doi:10.5194/acp-10-11707-2010.

Wesely, M. L. (1989), Parameterization of surface resistances to gaseous dry deposition in regional-scale numerical-models, *Atmos. Environ.*, *23*(6), 1293–1304, doi:10.1016/0004-6981(89)90153-4.

Wofsy, S. C., H. S. Team, T. Cooperating Modellers, and T. Satellite (2011), HIAPER Pole-to-Pole Observations (HIPPO): Fine-grained, global-scale measurements of climatically important atmospheric gases and aerosols, *Phil. Trans. Math. Phys. Eng. Sci.*, *369*(1943), 2073–2086, doi:10.1098/rsta.2010.0313.

Xiao, Y. P., D. J. Jacob, and S. Turquety (2007), Atmospheric acetylene and its relationship with CO as an indicator of air mass age, *J. Geophys. Res.*, *112*, D12305, doi:10.1029/2006JD008268.

Zarzycki, C. M., and T. C. Bond (2010), How much can the vertical distribution of black carbon affect its global direct radiative forcing?, *Geophys. Res. Lett.*, *37*, L20807, doi:10.1029/2010GL044555.

Zhang, X. Y., Y. Q. Wang, X. C. Zhang, W. Guo, and S. L. Gong (2008), Carbonaceous aerosol composition over various regions of China during 2006, *J. Geophys. Res.*, *113*, D14111, doi:10.1029/2007JD009525.

Zhang, Q., et al. (2009), Asian emissions in 2006 for the NASA INTEX-B mission, *Atmos. Chem. Phys.*, *9*(14), 5131–5153.